Probing Structure−Parameter Correlations in the Molten Salt Synthesis of $BaZrO_3$ Perovskite Submicrometer-Sized Particles

Hongjun Zhou,[†] Yuanbing Mao,[†,‡] and Stanislaus S. Wong*[,†,§]

Department of Chemistry, State University of New York at Stony Brook, Stony Brook, New York 11794-3400, and Materials and Chemical Sciences Department, Brookhaven National Laboratory, Building 480, Upton, New York 11973

Received May 29, 2007. Revised Manuscript Received July 18, 2007

Single-crystalline perovskite $BaZrO_3$ submicrometer-sized particles were synthesized using a simple, scaleable molten salt method. In this paper, in addition to a time-dependent particle evolution study, we explored primarily the effects of different experimental processing parameters, such as the identity of the salt, annealing temperatures, overall reaction times, cooling rates, and the chemical nature of the precursor in determining their impact upon the purity, size, shape, and morphology of the as-obtained products. We also discuss the role of additional experimentally controllable factors such as the heating rate applied, the amount of salt used, the molar ratios of precursors involved, and the use of surfactant. By a judicious choice of experimental parameters and conditions, we describe herein a rational means of producing pure products with a reproducible composition and morphology.

Introduction

The synthesis of complex ternary transition metal oxides, many of which possess a perovskite structure, is a major focal point of interest because a majority of these materials possesses a host of interesting physical properties with applications in fields ranging from ferroelectricity, ferromagnetism, piezoelectricity, pyroelectricity, and high-temperature superconductivity to optoelectronics.[1−3] Our group has expended significant effort in demonstrating that the molten salt synthesis (MSS) method, in particular, is one of the simplest, most versatile, and highly cost-effective approaches available for obtaining crystalline, chemically pure, single-phase nanoscale materials at lower temperatures and often in overall shorter reaction times with little residual impurities as compared to conventional solid-state reactions. The intrinsic scalability, flexibility, and facility of this technique render it attractive for the fabrication of a range of ternary metal oxides.

The fundamental basis[4] of molten salt reactions is the reliance on the use of inorganic molten salt as the reaction medium. Salt media used by other groups have ranged from the eutectic mixture of $AlCl_3$/NaCl/KCl with a relatively low melting point of 89 °C to cryolite or Na_3AlF_6 with a particularly high melting point of 1003 °C. Moreover, these salts often possess a host of favorable physicochemical properties such as a greater oxidizing potential, higher mass transfer, higher thermal conductivity, as well as relatively lower viscosities and densities, as compared to conventional solvents.[5] In fact, with MSS (i) the identity as well as the size of the anion associated with the salt, (ii) the nature of the solubility values as well as the dissolution rates of the constituent components within the molten salt itself, (iii) the precise melting point of either the salt or the complex salt mixture used, (iv) the heating temperature and duration, as well as (v) the unique morphological (e.g., shape) and chemical composition of the precursors involved are all important, readily controllable factors that influence the growth rate as well as the resultant structural characteristics (i.e., size, shape, and crystallinity) of the as-prepared particles.[4,6,7]

All of these experimental realities suggest, in theory, a high degree of tunability with respect to parameter selection for molten salt chemical reactions with the real possibility of generating large amounts of pure products with a predictable, reproducible morphology.[5,7,8] Thus, our fundamental motivation in this study has been to understand and probe parameter control in MSS reactions for the production of ternary metal oxide perovskite structures with reliable shape and size control. In this regard, we have had preliminary success with respect to the reliable synthesis and characterization of morphological motifs of $BaTiO_3$, $SrTiO_3$, and $Ca_{1-x}Sr_xTiO_3$ nanostructures.[9,10] We expect our protocols to have relevance for the rational synthesis of other types of metal oxides.

In this specific paper, we focus on the synthesis of barium zirconate ($BaZrO_3$), a cubic perovskite with a unit cell edge length of 4.19 Å. $BaZrO_3$ exhibits a high protonic conductiv-

* Corresponding author. Phone: (631) 632-1703; e-mail: sswong@notes.cc.sunysb.edu or sswong@bnl.gov.
† State University of New York at Stony Brook.
‡ Current address: Department of Chemical and Biomolecular Engineering, University of California at Los Angeles, Los Angeles, CA 90095.
§ Brookhaven National Laboratory.

(1) Zhang, S.; Randall, C. A.; Shourt, T. R. *J. Appl. Phys.* **2004**, *95*, 4291.
(2) Burscu, E.; Ravichandran, G.; Bhattacharya, K. *J. Mech. Phys. Solids* **2004**, *52*, 823.
(3) Zook, J. D.; Casselman, T. N. *Phys. Rev. Lett.* **1966**, *17*, 960.
(4) Hayashi, Y.; Kimura, T.; Yamaguchi, T. *J. Mater. Sci.* **1986**, *21*, 757.
(5) Volkov, S. V. *Chem. Soc. Rev.* **1990**, *19*, 21.
(6) Zboril, R.; Mashlan, M.; Petridis, D. *Chem. Mater.* **2002**, *14*, 969.
(7) Yoon, K. H.; Cho, Y. S.; Kang, D. H. *J. Mater. Sci.* **1998**, *33*, 2977.
(8) Bloom, H. *The Chemistry of Molten Salts*; W. A. Benjamin, Inc.: New York, 1967.
(9) Mao, Y.; Banerjee, S.; Wong, S. S. *J. Am. Chem. Soc.* **2003**, *125*, 15718.
(10) Mao, Y.; Wong, S. S. *Adv. Mater.* **2005**, *17*, 2194.

10.1021/cm071456j CCC: $37.00
Published on Web 10/05/2007

ity upon the addition of dopants, rendering it suitable for applications ranging from fuel cells to hydrogen sensors operated at high temperature.[11] Its high dielectric constant (30−40), its wide band gap (~5.3 eV), and its correspondingly high breakdown strength make this oxide material appropriate for use in high voltage and high reliability capacitive applications, such as electro-optic devices and multilayer capacitors.[12−14] Moreover, its high melting point (2600 °C) and its chemical stability at high temperatures render it suitable not only as a refractory material but also as a precursor in the production of high-quality, high T_c superconducting materials.[15] Finally, its sensitivity to humidity is useful for its application as a moisture sensor.[16]

A number of existing methods can be used to synthesize nanoscale $BaZrO_3$ particulates. Apart from freeze-drying,[17] many reported studies have relied on liquid-phase reactions such as sol−gel,[18,19] coprecipitation,[20] thermal decomposition,[21] and hydrothermal techniques[22−27] as well as conventional solid-state reactions[28,29] in addition to combinations thereof. Many of these reactions often involved either an additional sintering[30] or sonication (e.g., nanoparticle formation probed as a function of ultrasonicator output power and time)[31] step. $BaZrO_3$ particles can also be formed by the reaction[32] of very fine (70−90 nm) ZrO_2 powders and coarse (~1 μm) $BaCO_3$ powders in both dry as well as humid air using a temperature range of 900−1300 °C. Recently, the synthesis of nanoscale $BaZrO_3$ was initiated by urea-induced precipitation followed by a low-temperature thermal treatment.[33] A reported solvothermal method relied on the dissolution of either alkali or alkaline earth metals (e.g., Ba) in benzyl alcohol and a subsequent reaction with transition metal alkoxides (e.g., $Zr(OiPr)_4 \cdot HOiPr$) at low-temperature ranges from 200 to 220 °C for 3 days.[34] A typical hydrothermal[22−27] analogue to this reaction was associated with the reaction of $ZrOCl_2 \cdot 8H_2O$, $Ba(OH)_2$, and KOH to create a slurry (pH 13), which was then heated in an autoclave at 130 °C for 1 day. In addition, $BaZrO_3$ nanoparticles have been prepared by a reverse micelle process in which (i) barium nitrate and zirconium dinitrate oxide were used as precursor materials, (ii) sodium hydroxide was utilized as the precipitating agent, and (iii) *n*-octane, 1-butanol, and cetyl trimethylammonium bromide were dispersed together to form the desired microemulsion.[35] Last, a microwave-assisted preparation, run under ambient conditions, has been reported in which $BaCl_2 \cdot$hydrate was initially dissolved in ethylene glycol, reacted with KOH, and ultimately microwave refluxed in the presence of $ZrOCl_2$ for 2 h, all under a static pressure of N_2, to generate particles measuring ~200 nm × 600 nm.[36]

The novelty of our specific approach can be summarized as follows. To the best of our knowledge, this is the first study to systematically probe parameter control in the molten salt synthesis of submicrometer-sized perovskite particles with the aim of reliable and reproducible size, shape, and composition control. Second, whereas Gopalan et al.[37] have formed solid solutions of $BaZrO_3-SrZrO_3$ using the molten salt eutectic of NaOH−KOH as a solvent, no one has reported the synthesis of either nanometer- or micrometer-sized pristine $BaZrO_3$ particles using this particular eutectic solvent. Third, one of the few papers to deal with shape control in $BaZrO_3$ utilized a hydrothermal method under very high pH conditions to generate truncated rhombic dodecahedra and spheres with dimensions over 1 μm; shape control was achieved therein by changing the solvent polarity.[23] We have recently reported[38] on the narrow issue of controlling the percentage of cubes versus spheres in samples of $BaZrO_3$ generated by MSS. However, as compared with comprehensive papers dealing with shape control in liquid-phase reactions,[39,40] there are noticeably fewer analogous systematic reports associated with the broader and more generalized problem of parameter selection in the molten salt method.[41−43] We rectify this situation in this paper by isolating and analyzing the individual roles of salt medium, annealing temperatures, cooling rates, as well as precursor selection in determining overall product morphology, composition, size, and shape in a molten salt synthesis of crystalline submicrometer-sized perovskite particles.

(11) Yajima, T.; Suzuki, H.; Yogo, T.; Iwahara, H. *Solid State Ionics* **1992**, *51*, 101.
(12) Shende, R. V.; Krueger, D. S.; Rossetti, G. A.; Lombardo, S. J. *J. Am. Ceram. Soc.* **2001**, *84*, 1648.
(13) Macmanus-Driscoll, J. L.; Foltyn, S. R.; Jia, Q. X.; Wang, H.; Serquis, A.; Civale, L.; Maiorov, B.; Hawley, M. E.; Maley, M. P.; Peterson, D. E. *Nat. Mater.* **2004**, *3*, 439.
(14) Koenig, J.; Jaffe, B. *J. Am. Ceram. Soc.* **1964**, *47*, 87.
(15) Kang, S.; Leonard, K. J.; Martin, P. M.; Li, J.; Goyal, A. *Supercond. Sci. Technol.* **2007**, *20*, 11.
(16) Viviani, M.; Buscaglia, M. T.; Buscaglia, V.; Leoni, M.; Nanni, P. *J. Eur. Ceram. Soc.* **2001**, *21*, 1981.
(17) Badica, P.; Aldica, G.; Iyo, A.; Bradea, I.; Jaklovszky, J. *Mater. Lett.* **2003**, *58*, 250.
(18) Ling, H.; Li, A.; Wu, D.; Tang, Y.; Liu, Z.; Ming, N. *Mater. Chem. Phys.* **2002**, *75*, 170.
(19) Sin, A.; Montaser, B. E.; Odier, P.; Weiss, F. *J. Am. Ceram. Soc.* **2002**, *85*, 1928.
(20) Brzezinska-Miecznik, J.; Haberko, K.; Bucko, M. M. *Mater. Lett.* **2002**, *56*, 273.
(21) Kirby, N. M.; Van Riessen, A.; Buckley, C. E.; Wittorff, V. W. *J. Mater. Sci.* **2005**, *40*, 97.
(22) Lencka, M. M.; Nielsen, E.; Anderko, A.; Riman, R. E. *Chem. Mater.* **1997**, *9*, 1116.
(23) Lu, Z.; Tang, Y.; Chen, L.; Li, Y. *J. Cryst. Growth* **2004**, *266*, 539.
(24) Kutty, T. R. N.; Vivekanandan, R.; Philip, S. *J. Mater. Sci.* **1990**, *25*, 3649.
(25) Vivekanadan, R.; Philip, S.; Kutty, T. R. N. *Mater. Res. Bull.* **1987**, *22*, 99.
(26) Millot, N.; Xin, B.; Pighini, C.; Aymes, D. *J. Eur. Ceram. Soc.* **2005**, *25*, 2013.
(27) Kolen'ko, Y. V.; Burukhin, A. A.; Churagulov, B. R.; Oleinikov, N. N.; Vanetsev, A. S. *Inorg. Mater.* **2002**, *38*, 252.
(28) Azad, A.; Subramaniam, S. *Mater. Res. Bull.* **2002**, *37*, 85.
(29) Yamanaka, S.; Hamaguchi, T.; Oyama, T.; Matsuda, T.; Kobayashi, S.; Kurosaki, K. *J. Alloys Compd.* **2003**, *359*, 1.
(30) Robertz, B.; Boschini, F.; Cloots, R.; Rulmont, A. *Int. J. Inorg. Mater.* **2001**, *3*, 1185.
(31) Athawale, A. A.; Bapat, M. *J. Metastable Nanocryst. Mater.* **2005**, *23*, 3.
(32) Ubaldini, A.; Buscaglia, V.; Uliana, C.; Costa, G.; Ferretti, M. *J. Am. Ceram. Soc.* **2003**, *86*, 19.
(33) Boschini, F.; Robertz, B.; Rulmont, A.; Cloots, R. *J. Eur. Ceram. Soc.* **2003**, *23*, 3035.
(34) Niederberger, M.; Pinna, N.; Polleux, J.; Antonietti, M. *Angew. Chem., Int. Ed.* **2004**, *43*, 2270.
(35) Leonard, K. J.; Sathyamurthy, S.; Paranthaman, M. P. *Chem. Mater.* **2005**, *17*, 4010.
(36) Palchik, O.; Zhu, J.; Gedanken, A. *J. Mater. Chem.* **2000**, *10*, 1251.
(37) Gopalan, S.; Mehta, K.; Virkar, A. V. *J. Mater. Res.* **1996**, *11*, 1863.
(38) Zhou, H.; Mao, Y.; Wong, S. S. *J. Mater. Chem.* **2007**, *17*, 1707.
(39) Wiley, B.; Sun, Y.; Mayers, B.; Xia, Y. *Chem.—Eur. J.* **2005**, *11*, 454.
(40) Pileni, M.-P. *Nat. Mater.* **2003**, *2*, 145.
(41) Wang, Y.; Ma, J.; Tao, J.; Zhu, X.; Zhou, J.; Zhao, Z.; Xie, L.; Tian, H. *Mater. Sci. Eng., B* **2006**, *130*, 277.
(42) Ito, Y.; Shimada, S.; Inagaki, M. *J. Am. Ceram. Soc.* **1995**, *78*, 2695.
(43) Battisha, I. K.; Speghini, A.; Polizzi, S.; Agnoli, F.; Bettinelli, M. *Mater. Lett.* **2002**, *57*, 183.

Experimental Procedures

Synthesis. In a typical protocol, barium oxalate (Aldrich, 99.999%), ZrO_2 (Nanostructured and Amorphous Materials Inc., 40−50 nm, 99.9%), and the relevant salt/eutectic salt mixture were mixed in a molar ratio of 1:1:20 and ground for 10 min. The mixture was then placed within a porcelain combustion boat (Coors), which was subsequently inserted into a quartz tube and heated to the desired temperature at a rate of 5 °C/min, after which the product was isothermally annealed at the preset temperature. After being cooled to room temperature at a specified cooling rate, samples were subsequently washed with copious amounts of distilled water and heated at 80 °C overnight in a drying oven.

Characterization. *X-ray Diffraction (XRD).* Rapid determination of the product crystalline phase was deduced from XRD measurements. An initial approximation of sample purity was achieved without the use of any internal standard. Samples for analyses were prepared by grinding as-prepared powder thoroughly in ethanol using a mortar and pestle, followed by loading onto glass slides, and subsequent drying in air. Diffraction patterns were collected using a Scintag diffractometer, operating in the Bragg configuration using Cu K_α radiation ($\lambda = 1.54$ Å) from 20 to 65° at a scanning rate of 2°/min.

The weight percentage of $BaZrO_3$ in as-prepared samples was obtained via quantitative XRD (Q-XRD). For precise quantitative analysis, the scan rate utilized was 0.2°/min. Otherwise, parameters used for slit widths and accelerating voltages were identical for all samples. Quantitative analysis was achieved by employing a Rietveld refinement[44,45] through the mediation of GSAS and EXPGUI software;[44,46] this method is based on the fact that the intensity diffracted by a crystalline phase is essentially proportional to the quantity of the diffracting material. Hence, this protocol[45] relies on theoretically reconstructing the entire diffraction profile by gradual refinement of the relevant unit cell, structural parameters, and phase constituents. Structure models for various compounds used in the calculations including $BaCO_3$, ZrO_2, $BaZrO_3$, and $ZrSiO_4$ as well as crystallographic information files were obtained from the literature.[47−50] Calculated patterns were noted to fit reasonably well with measured data, from which precise weight percentages of the various chemical constituents could then be extracted. A typical refined pattern, shown in Supporting Information Figure S1, is provided as an example.

For samples requiring a more accurate quantitative analysis of composition, a known quantity of zirconium silicate ($ZrSiO_4$, Acros, 99%), which was utilized as an internal standard,[51] was carefully combined with as-prepared samples. That is, the exact amount of internal standard used was set at 25% by careful rendering of the final weight ratio of the internal standard to that of the as-prepared sample as 1:3.

X-ray Photoelectron Spectroscopy (XPS). Elemental analysis was obtained by XPS. Pressed wafers or cut sections of the samples were attached to stainless steel sample holders using conductive double-sided carbon tape and installed in the vacuum chamber of a Model DS800 XPS surface analysis system (Kratos Analytical Plc of Manchester). The chamber was evacuated to a base pressure of $\sim 5 \times 10^{-9}$ Torr. A hemispherical energy analyzer was used for electron detection. XPS spectra were collected using a magnesium K_α X-ray source at an 80 eV pass energy and in 0.75 eV steps for each sample survey spectrum. Integration and analysis of elemental peak areas in high-resolution spectra were used to generate estimates of the atomic and weight concentrations of the elements present in the samples.

Electron Microscopy. The particle size and morphology of the resulting as-prepared products were initially characterized using a field emission scanning electron microscopy instrument (FE-SEM Leo 1550), operated at an accelerating voltage of 15 kV and equipped with energy-dispersive X-ray spectroscopy (EDS) capabilities. Samples were deposited onto conductive carbon tapes, which were subsequently attached to the surfaces of SEM brass stubs. These samples were then conductively coated with gold by sputtering for 20 s to minimize charging effects under SEM imaging conditions.

Specimens for transmission electron microscopy (TEM) and high-resolution TEM (HRTEM) were obtained by drying droplets of $BaZrO_3$ samples from an ethanolic dispersion onto 300 mesh Cu grids, coated with a lacey carbon film. TEM images were taken at an accelerating voltage of 120 kV on a Philips CM12 instrument. HRTEM images and electron diffraction patterns were obtained on a JEOL 2010F HRTEM at an accelerating voltage of 200 kV. This instrument was equipped with an Oxford INCA EDS system with the potential of performing selected area electron diffraction (SAED) to further characterize the crystallinity of as-prepared $BaZrO_3$ particles.

Results and Discussion

On the basis of previous protocols we have developed for optimal shape control,[38] cubic $BaZrO_3$ particles (Figure 1a, edge length measuring 120 ± 25 nm based on a measurement of 50 particles) could be prepared by heating precursors in a NaOH−KOH mixture (49.2:50.8 mol %; mp 170 °C) to 720 °C. Annealing of this sample at this temperature ensued for 30 min, followed by subsequent quenching of this sample to room temperature at an average rate of 100 °C/min. Conversely, for spherical particles (Figure 1b, diameter of 320 ± 100 nm based on a measurement of 50 particles), mixtures were annealed for 3.5 h at 720 °C, followed by gradual in situ furnace cooling to room temperature at an average rate of 3.5 °C/min. Histograms showing size distributions for these differently shaped particles are highlighted in Supporting Information Figure S2.

XRD patterns and EDS spectra for the two sets of samples are identical within error as well as with expected results. Hence, a representative XRD pattern (Figure 1c) and an EDS spectrum (Figure 1d) are shown. The EDS spectrum confirms the presence of Ba, Zr, and O. In addition, the XRD peaks can be readily indexed to the cubic phase (space group: $Pm3m$) of $BaZrO_3$ with a calculated lattice constant of $a = 0.4183$ nm, in good agreement with literature ($a = 0.4181$ nm, JCPDS no. 06−0399). On the basis of our analysis of expected peak positions in XRD patterns reported throughout this entire paper, we are fairly confident that we have not formed either Ba_2ZrO_4 or $Ba_3Zr_2O_7$ in any measurably significant quantities. Supporting Information Figure S3 shows typical high-resolution XPS spectra. The Ba $3d_{3/2}$ and $3d_{5/2}$ peaks are located at 794.42 and 779.11 eV, respectively, whereas the Zr $3d_{3/2}$ and $3d_{5/2}$ peaks are situated at 183.23 and 180.87 eV, respectively.[52,53] These data are consistent

(44) Bish, D. L.; Howard, S. A. *J. Appl. Crystallogr.* **1988**, *21*, 86.
(45) Orlhac, X.; Fillet, C.; Deniard, P.; Dulac, A. M.; Brec, R. *J. Appl. Crystallogr.* **2001**, *34*, 114.
(46) Toby, B. H. *J. Appl. Crystallogr.* **2001**, *34*, 210.
(47) Smith, D. K.; Newkirk, W. *Acta Crsytallogr.* **1965**, *18*, 983.
(48) Robinson, K.; Gibbs, G. V.; Ribbe, P. H. *Am. Miner.* **1971**, *56*, 782.
(49) De Villiers, J. P. R. *Am. Miner.* **1971**, *56*, 758.
(50) Levin, I.; Amos, T. G.; Bell, S. M.; Farber, L.; Vanderah, T. A.; Roth, R. S.; Toby, B. H. *J. Solid State Chem.* **2003**, *175*, 170.
(51) Eckert, J. O., Jr.; Hung-Houston, C. C.; Gersten, B. L.; Lencka, M. M.; Riman, R. E. *J. Am. Ceram. Soc.* **1996**, *79*, 2929.

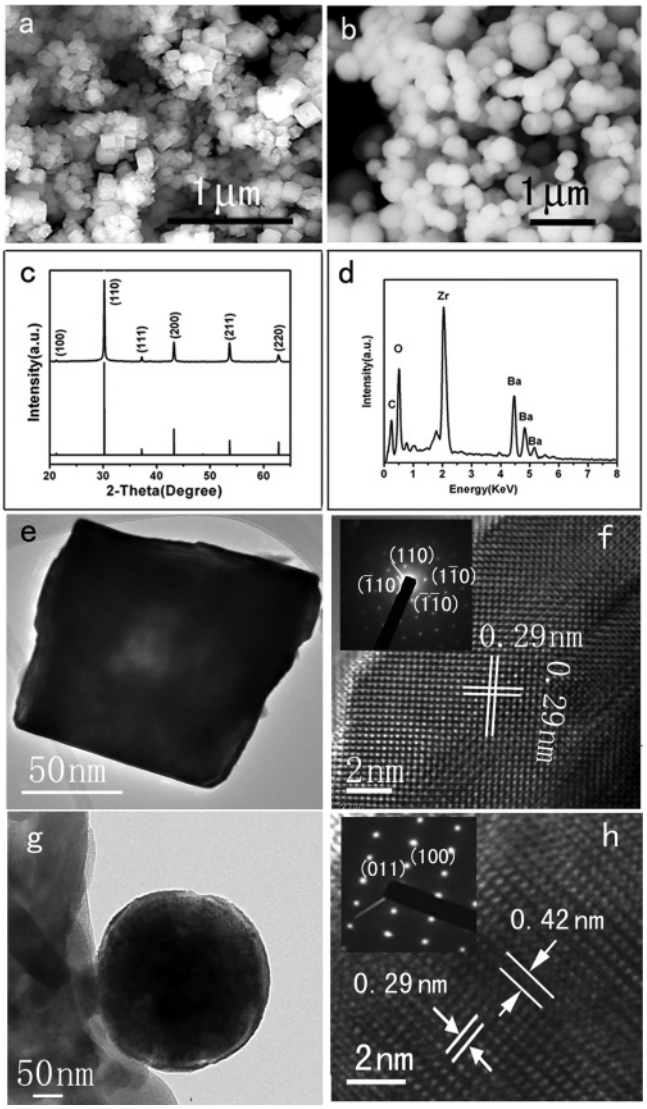

Figure 1. SEM images of as-prepared $BaZrO_3$ (a) cubes and (b) spheres. (c and d) XRD and EDS patterns of these samples, respectively. The lower pattern in panel c corresponds to a database standard (JCPDS 06-0399) for the cubic phase of $BaZrO_3$. The carbon peak in (d) originates from the conductive carbon tape. (e and f) TEM, HRTEM, and SAED pattern (inset) of a $BaZrO_3$ cube. (g and h) TEM, HRTEM, and SAED pattern (inset) of a $BaZrO_3$ sphere.

with the oxidation states of Ba and Zr, as being +2 and +4, respectively, which are expected of $BaZrO_3$ formation.

The TEM image (Figure 1e) shows the cubic morphology of a typical individual particle. The HRTEM image and associated SAED pattern obtained from the [001] projection (Figure 1f and the corresponding inset) suggest the single-crystalline nature of the particle with no apparent defects and dislocations. The spacing of the observed lattice fringes has been deduced to be 0.29 nm, which can be associated with the {110} plane of the cubic phase of $BaZrO_3$. By comparison with $BaZrO_3$ cubes, $BaZrO_3$ spheres (Figure 1g) are also single-crystalline with no apparent defects and dislocations. The spacings of observed lattice fringes are 0.29 and 0.42 nm, respectively, and have been correspondingly indexed to the {011} and {100} planes of the cubic phase of $BaZrO_3$ in agreement with the SAED pattern (inset of Figure 1h).

To demonstrate the effect of different reaction parameters with respect to phase purity and particle morphology of $BaZrO_3$, we performed a series of systematic experiments, as delineated in Table 1. Experimental variables were carefully crafted so that the behavior of the subsets of samples could be reliably compared across individual discrete parameters, with all other parameters kept constant.

As an example, when examining samples annealed at different temperatures (samples G−I), even though the times required to attain the desired annealing temperatures were different, overall reaction times remained constant. We accomplished this feat partly by quenching samples to room temperature at a very high average rate of 100 °C min^{-1} to minimize the possible time differential resulting from cooling, starting from these various different annealing temperatures.

Selection of Salt. As shown in Figure 2a, regardless of the overall reaction time, sample A, prepared in the absence of salt, contains not only $BaZrO_3$ but also impurity phases that can be attributed to $BaCO_3$ and ZrO_2. Although the decomposition temperature of $BaCO_3$ is expected to be around 821 °C,[54] the appearance of $BaCO_3$ may arise from either the recombination of CO_2 and BaO during the cooling process or the incomplete decomposition of barium oxalate.

A number of samples was subsequently prepared by running molten salt reactions above the melting points of various salt media tried. Hence, we note that the weight percentage of $BaZrO_3$ increased from 69% (sample A, no salt used) to 93.3% (sample D) in the presence of NaCl (Fisher; mp 801 °C) and to 93.9% (sample C) in a mixture of NaCl/KCl (50:50 mol % ratio; mp 658 °C) at an annealing temperature of 820 °C. In the presence of NaOH/KOH (49.2:50.8 mol % ratio; mp 170 °C) as the eutectic salt mixture, $BaZrO_3$ with a weight percentage of almost 100% could be generated at rather low temperatures (e.g., 720 °C); interestingly, this sample (sample B) remained compositionally stable even upon annealing to 820 °C. It is noteworthy that in salt media such as $NaNO_3$ (J.T. Baker Chemical Co.; mp 310 °C) and $NaNO_3$/NaCl (93.6:6.4 mol % ratio; mp 294.7 °C), comprising samples E and F, from the XRD patterns, no $BaZrO_3$ was synthesized at all, even at the same overall reaction times as the other samples and even after annealing at 320 °C. It should be noted that we did not proceed to higher annealing temperatures (such as 700−800 °C) in these specific systems because salts such as $NaNO_3$ will decompose above 380 °C. Nonetheless, overall, the apparent lack of $BaZrO_3$ particle formation using nitrate salts was a surprising result because there have been reports of perovskite particle aggregate formation in the presence of molten alkali metal oxonitrates.[55]

(52) Fuenzalida, V. M.; Pilleux, M. E. *J. Mater. Res.* **1995**, *10*, 2749.
(53) Lyapin, A.; Juergens, L. P. H.; Graat, P. C. J.; Mittemeijer, E. J. *Surf. Interface Anal.* **2004**, *36*, 989.
(54) Barin, I.; Knacke, O. *Thermochemical Properties of Inorganic Substances*; Springer-Verlag: New York, 1973.
(55) Deloume, J.-P.; Scharff, J.-P.; Marote, P.; Durand, B.; Abou-Jalil, A. *J. Mater. Chem.* **1999**, *9*, 107.

Table 1. $BaZrO_3$ Samples Systematically Prepared with Different Processing Parameters at a Constant Heating Rate of 5 °C/Min[a]

parameter varied	sample	precursors	salt	annealing temp (°C)	time required to attain desired annealing temp (min)	time sample was maintained at desired annealing temp (min)	overall reaction time (min)	cooling rate (°C/min)	product description (obsd compound; percent purity; average particle size; morphology distribution)
salt	A	BaC_2O_4, ZrO_2	**no salt**	820	160	190	350	3.5	$BaZrO_3$ (69%; aggregates) with $BaCO_3$ and ZrO_2
	B	BaC_2O_4, ZrO_2	**NaOH/KOH**	720	140	210	350	3.5	$BaZrO_3$ (100%; ~320 nm; 100% spheres)
	C	BaC_2O_4, ZrO_2	**NaCl/KCl**	820	160	190	350	3.5	$BaZrO_3$ (93.9%; ~200 nm; cubes) with $BaCO_3$ and ZrO_2
	D	BaC_2O_4, ZrO_2	**NaCl**	820	160	190	350	3.5	$BaZrO_3$ (93.3%; ~200 nm; cubes) with $BaCO_3$ and ZrO_2
	E	BaC_2O_4, ZrO_2	**$NaNO_3$**	320	60	290	350	3.5	no $BaZrO_3$; impurities of $BaCO_3$ and ZrO_2
	F	BaC_2O_4, ZrO_2	**$NaNO_3$/NaCl**	320	60	290	350	3.5	no $BaZrO_3$; impurities of $BaCO_3$ and ZrO_2
annealing temp	G	BaC_2O_4, ZrO_2	NaOH/KOH	**520**	100	250	350	100	$BaZrO_3$ (84%; ~422 nm; 50% cubes/50% spheres) with $BaCO_3$ and ZrO_2
	H	BaC_2O_4, ZrO_2	NaOH/KOH	**620**	120	230	350	100	$BaZrO_3$ (95%; ~350 nm; 35% cubes/65% spheres) with $BaCO_3$ and ZrO_2
	I	BaC_2O_4, ZrO_2	NaOH/KOH	**720**	140	210	350	100	$BaZrO_3$ (100%; ~310 nm; 5% cubes/95% spheres)
annealing time	J	BaC_2O_4, ZrO_2	NaOH/KOH	720	140	30	**170**	100	$BaZrO_3$ (100%; ~120 nm; 100% cubes)
	K	BaC_2O_4, ZrO_2	NaOH/KOH	720	140	60	**200**	100	$BaZrO_3$ (100%; ~160 nm; 80% cubes/20% spheres)
	L	BaC_2O_4, ZrO_2	NaOH/KOH	720	140	120	**260**	100	$BaZrO_3$ (100%; ~265 nm; 30% cubes/70% spheres)
	I	BaC_2O_4, ZrO_2	NaOH/KOH	720	140	210	**350**	100	$BaZrO_3$ (100%; ~310 nm; 5% cubes/95% spheres)
	M	BaC_2O_4, ZrO_2	NaOH/KOH	520	100	70	**170**	100	$BaZrO_3$ (29%; ~211 nm; 90% cubes/10% spheres) with $BaCO_3$ and ZrO_2
	N	BaC_2O_4, ZrO_2	NaOH/KOH	520	100	100	**200**	100	$BaZrO_3$ (45%; ~222 nm; 85% cubes/15% spheres) with $BaCO_3$ and ZrO_2
	O	BaC_2O_4, ZrO_2	NaOH/KOH	520	100	160	**260**	100	$BaZrO_3$ (67%; ~297 nm; 75% cubes/25% spheres) with $BaCO_3$ and ZrO_2
	G	BaC_2O_4, ZrO_2	NaOH/KOH	520	100	250	**350**	100	$BaZrO_3$ (84%; ~422 nm; 50% cubes/50% spheres) with $BaCO_3$ and ZrO_2
influence of cooling rate	G	BaC_2O_4, ZrO_2	NaOH/KOH	520	100	250	350	**100**	$BaZrO_3$ (84%; ~422 nm; 50% cubes/50% spheres) with $BaCO_3$ and ZrO_2
	P	BaC_2O_4, ZrO_2	NaOH/KOH	520	100	250	350	**3.5**	$BaZrO_3$ (100%; ~450 nm; 40% cubes/60% spheres)
	J	BaC_2O_4, ZrO_2	NaOH/KOH	720	140	30	170	**100**	$BaZrO_3$ (100%; ~120 nm; 100% cubes)
	Q	BaC_2O_4, ZrO_2	NaOH/KOH	720	140	30	170	**3.5**	$BaZrO_3$ (100%; ~200 nm; 50% cubes/50% spheres)
	L	BaC_2O_4, ZrO_2	NaOH/KOH	720	140	120	260	**100**	$BaZrO_3$ (100%; ~265 nm; 30% cubes/70% spheres)
	R	BaC_2O_4, ZrO_2	NaOH/KOH	720	140	120	260	**3.5**	$BaZrO_3$ (100%; ~300 nm; 100% spheres)
nature of precursor	B	**BaC_2O_4, ZrO_2**	NaOH/KOH	720	140	210	350	3.5	$BaZrO_3$ (100%; ~320 nm; 100% spheres)
	S	**BaO, ZrO_2**	NaOH/KOH	720	140	210	350	3.5	$BaZrO_3$ (100%; ~490 nm; 100% spheres)
	T	**$BaCO_3$, ZrO_2**	NaOH/KOH	720	140	210	350	3.5	$BaZrO_3$ (100%; ~340 nm; 100% spheres)
	U	**$BaCl_2$, ZrO_2**	NaOH/KOH	720	140	210	350	3.5	$BaZrO_3$ (67%; aggregates) with $BaCO_3$ and ZrO_2
	V	**$Ba(NO_3)_2$, ZrO_2**	NaOH/KOH	720	140	210	350	3.5	$BaZrO_3$ (71%; aggregates) with $BaCO_3$ and ZrO_2
	W	**$Ba(OOCCH_3)_2$, ZrO_2**	NaOH/KOH	720	140	210	350	3.5	$BaZrO_3$ (75%; ~300 nm; 100% spheres) with $BaCO_3$ and ZrO_2
	X	**BaC_2O_4, $ZrOCl_2 \cdot 8H_2O$**	NaOH/KOH	720	140	210	350	3.5	$BaZrO_3$ (76%; aggregates) with $BaCO_3$ and ZrO_2

[a] Variables controllably altered in each series are in bold.

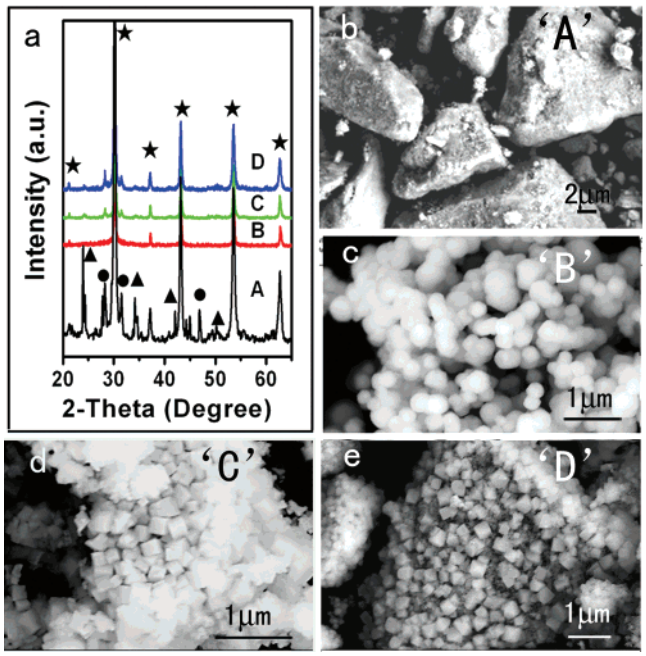

Figure 2. Selection of salt. (a) XRD patterns of samples A−D from Table 1, prepared using a molten medium containing no salt, NaOH/KOH, NaCl/KCl, and NaCl, respectively. (★, ▲, and ● represent reflection peaks associatd with $BaZrO_3$, $BaCO_3$, and ZrO_2, respectively). (b−e) Associated SEM images of samples A−D, respectively.

What is the effect of salt selection and of temperature? Molten salt solutions[56] can actually partake ofseveral functions. They can either catalyze reactions,[57] participate in reactions themselves by consuming reagents,[58] or merely act as a non-interfering solvent for the reagents.[9] However, in every case, the intrinsic solubilities of individual precursor molecules within these particular solvents are critical.

Thus, although salts such as $NaNO_3$ and $NaNO_3$/NaCl possess relatively low melting temperatures (∼200−300 °C), few precursor molecules of the different reacting species will adequately dissolve and diffuse in these particular solvents under such conditions, meaning that the corresponding reaction rates are low. Therefore, little, if any, $BaZrO_3$ forms. By contrast, at high temperatures such as ∼800 °C, in the presence of NaCl, precursor molecules will more readily disperse, dissociate, rearrange, and then diffuse rapidly throughout the salt, forming a reasonably homogeneous solution that fosters rapid reaction. Higher temperatures therefore not only increase the flux and mobility of reactive components but also imply a lower viscosity within the reaction medium, all of which is consistent with a higher rate of reactivity.[8] Thus, overall, as compared to samples prepared in the absence of salt (e.g., sample A), it is evident that the presence of either a chloride or a hydroxide salt medium encouraged the formation of $BaZrO_3$ (e.g., samples B−D).

The effect of using a hydroxide salt can be summarized as follows. It turns out that the hydroxide ion can actively participate in the reaction itself. For instance, it has been shown that molten hydroxide solutions[58] will not only react with metallic salts but also with metal oxides present. A plausible formation scheme (e.g., sample B) for $BaZrO_3$ is given in the presence of NaOH as the salt medium. KOH yields soluble K_2CO_3 as a byproduct, but otherwise the analysis is exactly the same as with NaOH alone.

$$BaC_2O_4 + 2NaOH + ZrO_2 \rightarrow Na_2CO_3 + BaZrO_3 + H_2O + CO \quad (1)$$

In the absence of hydroxide ion (e.g., sample E), a correspondingly viable reaction scheme is proposed as

$$BaC_2O_4 + ZrO_2 \rightarrow BaZrO_3 + CO + CO_2 \quad (2)$$

We have calculated the thermodynamic Gibbs' free energies for each of these reactions at increasing annealing temperatures, as shown in Table 2.[54] There are two trends worth noting. First, as expected, as the temperature progresses from 520 to 720 °C, the corresponding free energy values effectively double in magnitude, which is conducive to $BaZrO_3$ formation at higher temperatures. Second, the free energy values in the presence of hydroxide ion are ∼100 kJ/mol more favorable for the reaction to occur; for instance, at 720 °C, the free energy value for $BaZrO_3$ synthesis is approximately −439 kJ/mol in the presence of hydroxide ions, whereas in the absence of hydroxide ions, the corresponding free energy value is −341 kJ/mol. The large apparent difference in free energy of reaction coupled with the relatively high solubility and reactivity of metal species in hydroxide media can therefore explain the relative ease and overall completeness of $BaZrO_3$ formation that we have observed.

The nature of the salt medium also has an impact on the morphology of the as-prepared products; Ito et al. demonstrated this assertion in the synthesis of $PbTiO_3$ particles wherein cubic and rectangular particles were produced in the presence of KCl and LiF, respectively.[42,59] A similar effect was observed in our own experiments, shown in Figure 2b−e. In the absence of salt, products aggregated as large agglomerates (Figure 2b). In chloride-containing media, cubic particles were obtained (Figure 2d,e), whereas spherical particles were more readily found in hydroxide-containing media (Figure 2c). The shape of a nanocrystal (i.e., the reason for the morphology difference) is often determined by the relative specific surface energies associated with the facets of the growing crystal. As supporting evidence, we note the presence of different crystalline surface planes formed, when we compare the TEM images of as-prepared $BaZrO_3$ cubes versus spheres in Figure 1f,h. Hence, it is likely that the preferential adsorption of molecules and ions, such as chloride versus hydroxide, to different crystal faces likely directs the growth of nanoparticles to their ultimate product morphology by controlling relative growth rates associated with the different crystal faces.[60−62] This effect is analogous to the use of surfactants in other synthetic systems to achieve shape control.[63,64]

(56) Mamantov, G.; Braunstein, J., Eds. *Advances in Molten Salt Chemistry*; Plenum Press: New York, 1973; Vol. 4.
(57) Sundermeyer, W. *Chem. Ber.* **1964**, *97*, 1069.
(58) Liu, H.; Hu, C.; Wang, Z. L. *Nano Lett.* **2006**, *6*, 1535.
(59) Ito, Y.; Jadidian, B.; Allahverdi, M.; Safari, A. Particle Shape Control of Molten Salt Synthesized Lead Titanate. *Proceedings of the 2000 IEEE International Symposium on Applications of Ferroelectrics*, Honolulu, HI, July 21−Aug 2, 2000; Institute of Electrical Engineers: New York, 2000; Vol. 1, p 389.
(60) Murphy, C. J. *Science* **2002**, *298*, 2139.
(61) Puntes, V. F.; Krishnan, K. M.; Alivisatos, A. P. *Science* **2001**, *291*, 2115.
(62) Filankembo, A.; Giorgio, S.; Lisiecki, I.; Pileni, M. P. *J. Phys. Chem. B* **2003**, *107*, 7492.
(63) Xia, Y.; Yang, P.; Sun, Y.; Wu, Y.; Mayers, B.; Gates, B.; Yin, Y.; Kim, F.; Yan, H. *Adv. Mater.* **2003**, *15*, 353.
(64) Lee, S.-M.; Cho, S.-N.; Cheon, J. *Adv. Mater.* **2003**, *15*, 441.

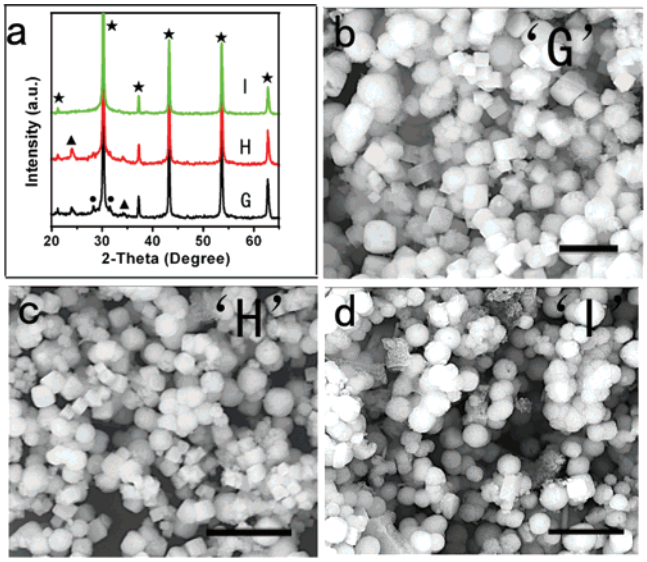

Figure 3. Annealing temperature. (a) XRD patterns of samples G, H, and I from Table 1. (★, ▲, and ● represent $BaZrO_3$, $BaCO_3$, and ZrO_2, respectively. (b−d) Corresponding SEM images of samples G, H, and I, respectively (i.e., in order of increasing annealing temperatures from 520 to 720 °C). Scale bar = 1 μm.

Table 2. Gibbs' Free Energy of Formation Values for Reactions 1 and 2 Regarding $BaZrO_3$ Particle Formation

annealing temp (°C)	reaction 1 (presence of hydroxide ion in molten salt media) (kJ/mol)	reaction 2 (absence of hydroxide ion in molten salt media) (kJ/mol)
520	−263	−153
620	−320	−214
720	−379	−277
820	−439	−341

Another key point has been the dispersibility factor. Because of the relatively high viscosity of hydroxide,[58] as-prepared particles grown in hydroxide media tend to be more dispersed and isolated than those fabricated in chloride media. Thus, the use of different salt species not only has an impact on the ease of reaction but also correlates with the morphology of the as-prepared product. We should mention that since hydroxide media tend to yield the best samples in terms of purity, morphology, and dispersion, the remainder of the paper will primarily focus on samples prepared using this medium with careful and rational control over a number of other different variables.

Annealing Temperature. As we have previously noted, the solubility and reactivity of precursors increase with the increasing annealing/reaction temperature of the solvent medium itself. Moreover, it is known that the viscosity of the molten salt decreases rapidly with an increase of temperature, thereby greatly facilitating the diffusion of precursor species in the solvent itself.[8] These effects have been studied in the series of samples G−I, which had been annealed at 520, 620, and 720 °C, respectively, with constant overall reaction times (350 min) and rapid cooling rates (100 °C/min). Associated data are shown in Figure 3. From XRD data, we note that the weight percentage of $BaZrO_3$ in these samples correlates well with increasing annealing temperature, starting from 84% (sample G) to 95% (sample H). Essentially no impurity phase was detected at the highest temperature, 720 °C (sample I), implying higher rates of reactivity and essentially full conversion to $BaZrO_3$ at the highest annealing temperatures.

Another key issue is product morphology. Whereas sample B, which had been slowly cooled to room temperature from an annealing temperature of 720 °C, resulting in an effectively longer reaction time, consisted of ∼100% spherical particles, samples G−I, which had been rapidly quenched, possessed varying percentages of cubes and spheres. In fact, the percentage of spheres increased from 50% in sample G to 65% in sample H and finally to 95% in sample I with increasing annealing temperature. Hence, these initial observations, which are consistent with our previous data,[38] suggest that higher annealing temperatures and longer overall reaction times are conducive to the production of relatively pure, spherically shaped $BaZrO_3$ samples.

Impact of Overall Reaction Time. To explore the effect of overall reaction times more thoroughly, samples J−L and I were prepared at an identical temperature (i.e., 720 °C) but with different annealing times and overall reaction times (e.g., ranging from 170 to 350 min). All of these samples contained ∼100 wt % $BaZrO_3$ with no detectable impurity, on the basis of XRD analysis.

In terms of morphology, as shown in Figure 4, sample J, synthesized with the least amount of reaction time (170 min), contained primarily cubes. As the overall annealing/reaction time was systematically increased, the percentage of spheres also increased from 20% in sample K (200 min of reaction time) to 70% in sample L (260 min of reaction time). Ultimately, in sample I, fabricated with a reaction time of 350 min, the proportion of spheres was ∼95%. Simultaneously, the average diameter of particles increased accordingly from 120 nm for sample J, 160 nm for sample K, 265 nm for sample L, and finally to 310 nm for sample I. Hence, it was evident that with an increasing annealing time, the samples progressed from cubes to spheres with a corresponding, simultaneous increase in particle size.

A parallel sample series (e.g., G and M− O) was prepared by annealing at a lower temperature (520 °C), while systematically varying overall reaction times from 170 to 350 min. From the XRD data shown in Supporting Information Figure S4, the weight percentage of the $BaZrO_3$ phase increased from 29% in sample M, synthesized after reaction for 170 min, to as much as 84% in sample G, produced after 350 min of annealing. We also observed an analogous increase in diameter as well as in the percentage of spheres in samples that had undergone additional annealing. That is, we progressed from ∼10% spheres in sample M to ∼50% spheres in sample G, supportive of the assertion that the conversion rate from cubes to spheres is favored at higher annealing temperatures.[38] In this span of samples, average particle diameters increased from ∼211 nm to as much as ∼422 nm, suggesting that increasing annealing times favor particle growth.

Influence of Cooling Rates. In the vast majority of papers[9,10,65] dealing with MSS either a slow cooling rate or an unimpeded furnace cooling is utilized. By contrast, in other techniques, such as coprecipitation, quenching (i.e., the idea of a very rapid cooling) is frequently used to control

(65) Park, T.-J.; Wong, S. S. *Chem. Mater.* **2006**, *18*, 5289.

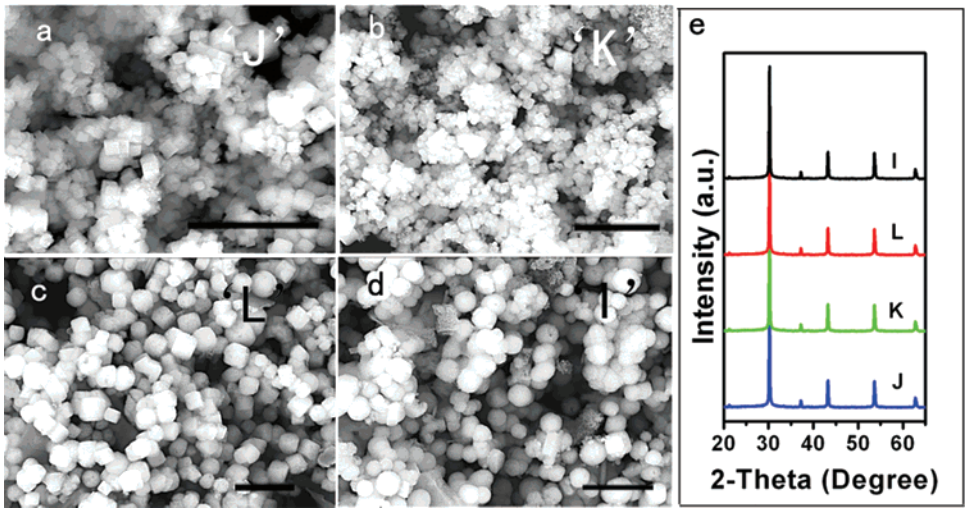

Figure 4. Impact of overall reaction time. Annealing performed at 720 °C. (a−d) SEM images of samples J−L and I, described in Table 1 (i.e., in order of increasing overall reaction times from 170 to 350 min). Scale bar = 1 μm. (e) Corresponding XRD patterns of samples J−L and I.

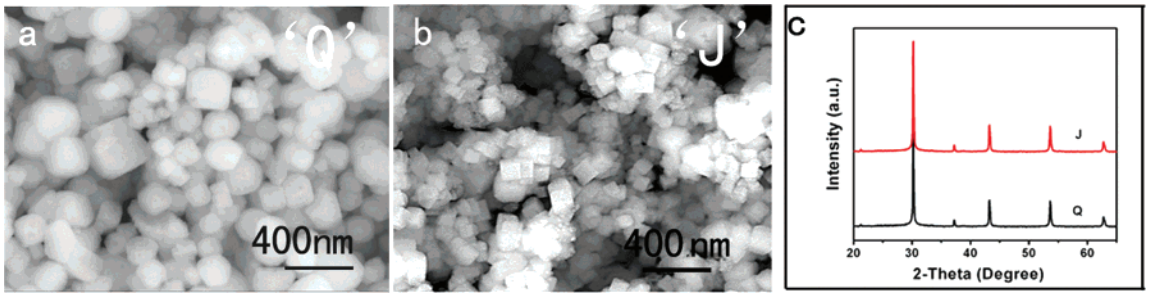

Figure 5. Influence of cooling rates. SEM images of samples (a) Q and (b) J, respectively. (c) Corresponding XRD patterns of samples Q and J, cooled at 3.5 and 100 °C/min, respectively.

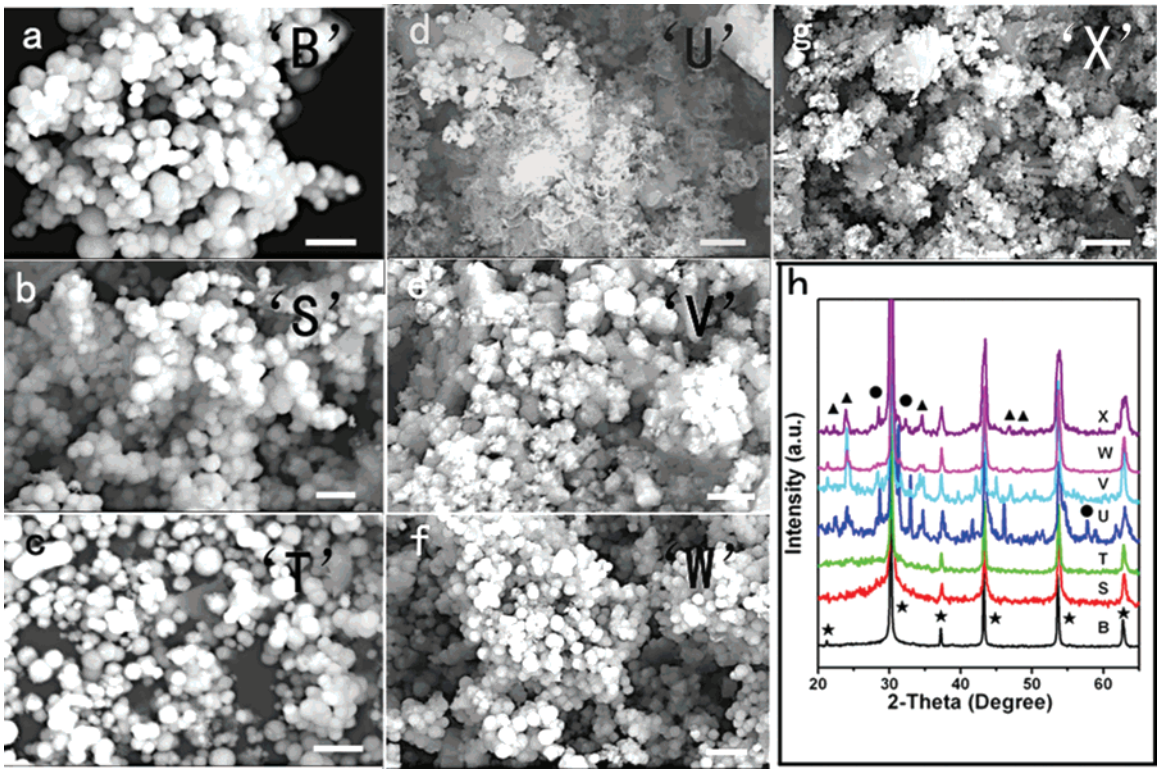

Figure 6. Choice of precursors. (a−g) SEM images of samples B and of S−X, respectively, prepared using a range of barium and zirconium precursors. Scale bar in each image = 1 μm. (h) Corresponding XRD patterns of these samples. Scale bar in microscopy images = 1 μm. ★, ▲, and ● represent reflection peaks associated with $BaZrO_3$, $BaCO_3$, and ZrO_2, respectively.

not only nucleation but also the subsequent growth, formation, and morphology of product particles.

Herein, we studied the effect of cooling rates in molten salt systems by comparing samples prepared by varying

quenching rates. For instance, sample P (~450 nm) was synthesized under exactly the same conditions as sample G (~422 nm), with the exception that the former was cooled at a rate of 3.5 versus 100 °C/min. However, sample P was essentially 100% pure, whereas sample G still possessed a detectable level of impurity (Supporting Information Figure S3). Thus, decreasing the cooling rate had the practical effect of increasing the overall reaction time, thereby allowing for improved sample quality.

As we noted earlier, an increased annealing time favored the formation of spheres in the products. The overall reaction time for the second pair of samples tested was 170 min. Hence, sample J (~120 nm), cooled at a rapid rate of 100 °C/min embodied almost exclusively cubes, whereas sample Q (~200 nm), prepared identically but cooled at a slower rate of 3.5 °C/min, contained a mixture of cubes and spheres (Figure 5). The overall reaction time for the third pair of samples tested was 260 min. Sample R (~300 nm) cooled at a rate of 3.5 °C/min was characterized by spheres. By contrast, sample L (~265 nm), prepared identically but cooled at a rate of 100 °C/min, was more heterogeneous with a noticeable quantity of cubes in addition to spheres.

In every case, samples that had been more slowly quenched at 3.5 °C/min tended to possess larger particles on average than those samples that had been more rapidly quenched at 100 °C/min. In addition, at any given annealing temperature, a slower cooling rate promotes the formation of spheres within the sample. Overall, these observations can be explained as follows. Both longer annealing times and higher annealing temperatures are conducive to the production of larger $BaZrO_3$ particles. Therefore, our results demonstrate that quenching in and of itself can be viably used in molten salt systems as a rational synthetic parameter not only to control particle growth but also to generate particles of a specific morphology, which could not otherwise be obtained under standard cooling conditions.[38]

Choice of Precursors. From Figure 6, we noted that replacing barium oxalate (sample B) with either barium oxide (sample S) or barium carbonate (sample T) also yielded samples possessing a relatively high purity as well as a uniform monodisperse spherical morphology. Similarly, sample W, synthesized using barium acetate, is composed of a large proportion of spherical particles, as was the case with samples B, S, and T, but was observed to possess significant oxide impurities, such as $BaCO_3$ and ZrO_2. By contrast, samples synthesized with either chloride- or nitrate-containing precursors of barium and of zirconium (samples U, V, and X) not only tended to be relatively impure with the presence of $BaCO_3$ and ZrO_2 but also were composed of large particle aggregates, measuring 1 to 2 μm.

What could explain this? Thermodynamically speaking, by altering the chemical identity of the precursors, we changed the values of the Gibbs' free energies of reactions in a corresponding fashion. For example if we compare the precursor choice of $BaCl_2$, $Ba(NO_3)_2$, and barium oxalate at 720 °C, the corresponding Gibbs' free energies of reactions are computed to be −93, −80, and −379 kJ/mol, respectively. The large magnitude of the free energy parameter associated with barium oxalate clearly suggests that it is a highly favorable reaction, and the purity of our products supports that assertion. However, it should be noted that high-quality $BaZrO_3$ particles were formed using BaO and $BaCO_3$ as precursors, even though the Gibbs' free energies for these reactions were −50 and −54 kJ/mol, respectively. Hence, it is expected that the reasons for the observed differences in purity and morphology as a function of precursor are not necessarily solely thermodynamic but rather are also dependent on a number of other factors including solubility, diffusion, and transport of reagent species within the reaction medium, all of which suggest a kinetic explanation for our observations.

Additional Factors. We have unpublished results demonstrating that a number of other factors likely play a role in morphology, purity, and composition. First, the addition of surfactant does not necessarily aid in enhancing product purity but in fact may simply assist in dispersing the product powder. Second, the amount of salt used in the reaction is also significant; the addition of excess salt can decrease impurity levels by favoring full dissolution and solubilization of precursors and subsequent precipitation of nuclei of the perovskite phase. In fact, perovskite particles have been noted to increase in size with increasing relative salt content.[7,66] Third, we have previously shown[67] that the relative molar ratio of precursors either with or without surfactant could control the aspect ratio of as-prepared $Bi_2Fe_4O_9$ submicrometer-sized particles. That is, whereas the use of a 1:1 molar ratio of Bi^{3+}/Fe^{3+} precursors generated smaller particles with cubic-like features, the highest molar ratio employed (i.e., 6:1 molar ratio of Bi^{3+}/Fe^{3+}) yielded larger structures with rod-like, rectangular shapes. Our preliminary results with $BaZrO_3$ are suggestive of a similar behavior in this system. Fourth, overly high heating rates will increase the quantity of impurities, likely because of nonoptimized reaction kinetics. Fifth, even the nature of the combustion boat may conceivably affect the purity of the product. For instance, we have noted that hydroxide media can potentially react with the porcelain boat itself. Moreover, in our samples, on average, 1.41% Na and 2.28% K were found, based on XPS results (Supporting Information Figure S5). A preliminary analysis of as-obtained EDS results, in support of the presence of impurities, suggests that there is ~1.81% Na and ~1.12% K in our samples. We note that the structural character of our samples (namely, the fact that our particles are relatively small and particulate in nature) can impact the accuracy of EDS data and may account for the numerical discrepancies observed relative to that of the XPS data. Nonetheless, overall, based on the spectroscopic data, it is reasonable to ascribe the appearance of Na and K to residues from the salt mixture and the additional presence of Si to the reaction crucible itself (Supporting Information Figure S5). We cannot fully discount the possible formation of either sodium silicate or potassium silicate, although it was likely to be insignificant. Any C observed would have resulted from

(66) Yoon, K. H.; Cho, Y. S.; Lee, D. H.; Kang, D. H. *J. Am. Ceram. Soc.* **1993**, *76*, 1373.
(67) Park, T.-J.; Papaefthymiou, G. C.; Moodenbaugh, A. R.; Mao, Y.; Wong, S. S. *J. Mater. Chem.* **2005**, *15*, 2099.

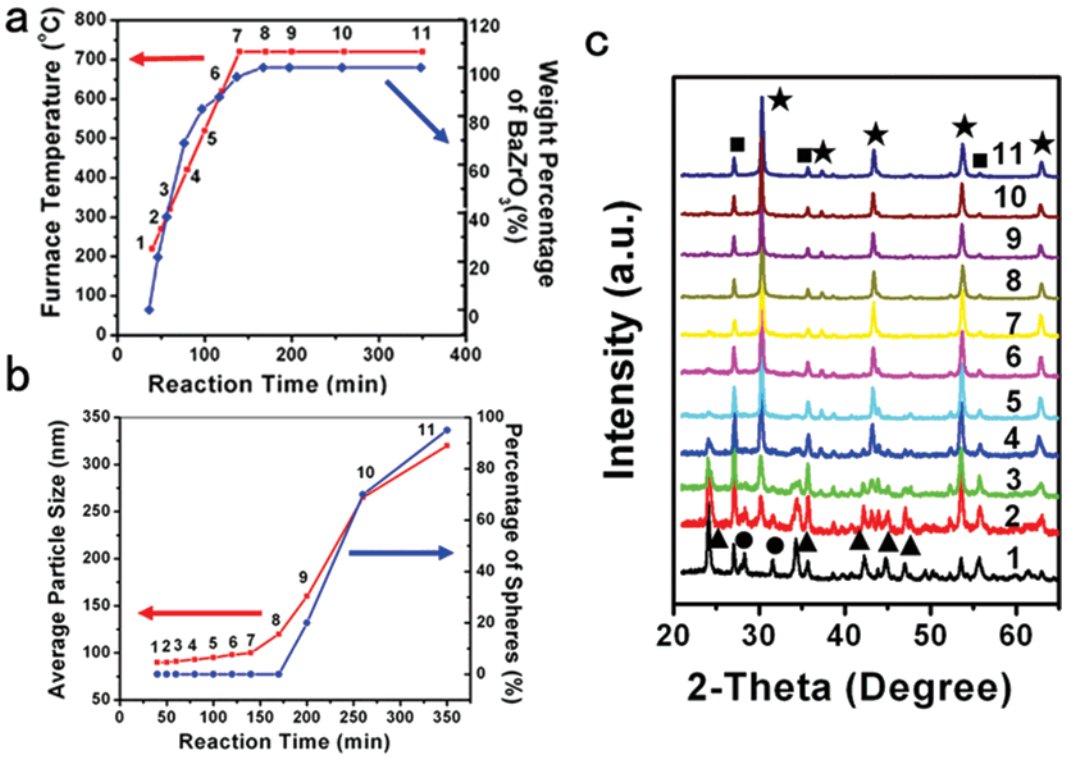

Figure 7. Time-dependent particle evolution. (a, b) Furnace temperature, wt% $BaZrO_3$, average particle size, and percentage of spheres of samples 1−11 plotted as a function of overall reaction time at a constant heating rate of 5 °C/min. Lines connecting data points are intended for visual guidance only. (c) Corresponding XRD patterns of samples 1−11 upon mixing with a constant amount of $ZrSiO_4$ used as an internal standard. (★, ▲, ●, and ■ represent $BaZrO_3$, $BaCO_3$, ZrO_2, and $ZrSiO_4$, respectively.)

Table 3. Samples Corresponding to Sequential Growth Stages of Sample I (Ultimately Annealed at 720 °C for 210 Min at a Constant Heating Rate of 5 °C/Min)[a]

sample	annealing temp (°C)	time required to reach desired annealing temp (min)	time sample was maintained at desired annealing temp (min)	overall reaction time (min)	average particle size (nm)	percentage of spheres	wt % $BaZrO_3$
1	220	40	0	40		0	∼0
2	270	50	0	50	90	0	∼21.7
3	320	60	0	60	91	0	∼38.4
4	420	80	0	80	93	0	∼68.8
5	520	100	0	100	95	0	∼82.9
6	620	120	0	120	98	0	∼87.9
7	720	140	0	140	100	0	∼96.1
8	720	140	30	170	120	0	∼100
9	720	140	60	200	160	20	∼100
10	720	140	120	260	265	70	∼100
11	720	140	210	350	320	95	∼100

[a] For all samples, precursors used included BaC_2O_4 and ZrO_2 in the presence of a NaOH/KOH salt medium. The cooling rate was kept constant throughout at ∼100 °C/min.

contaminant sources such as CO_2 physisorbed on the surface of BaO.[10]

Mechanistic Insights: Time-Dependent Particle Formation. To gain insights into the mechanism of $BaZrO_3$ particle formation in the presence of NaOH/KOH, a series of samples (1−11) corresponding to successive temporal growth stages during the formation of sample I (which had been annealed at 720 °C for 210 min) was synthesized. Descriptions are shown in Figure 7a,b as well as in Table 3, with samples 8−11 in Table 3 corresponding to samples J−L and I from Table 1. Rod-like motifs, as shown by arrows in Figure 8a,b and Supporting Information Figure S6a,b, initially appeared in samples 1−4, at reaction temperatures ranging from 220 to 420 °C, and may be attributable to the formation of barium carbonate.[68] EDS analysis for all samples was consistent with the presence of Ba, Zr, O, and C peaks, as expected. It should be noted that the ratio of intensities of the Zr versus Ba signals (Supporting Information Figure S7) ascribed to as-prepared rods was considerably lower than that for the corresponding, analogous particles, implying that these rods may have consisted of a mixture of ZrO_2, BaO, and $BaCO_3$.

Weight percentages of $BaZrO_3$ of these samples have been calculated, based on the XRD patterns shown in Figure 7c. Average particle sizes and percentages of spheres within samples were obtained from SEM images shown in Figure 8 and Supporting Information Figure S6. Sample 1, quenched

(68) Wang, L.; Zhu, Y. *Chem. Lett.* **2003**, *32*, 594.

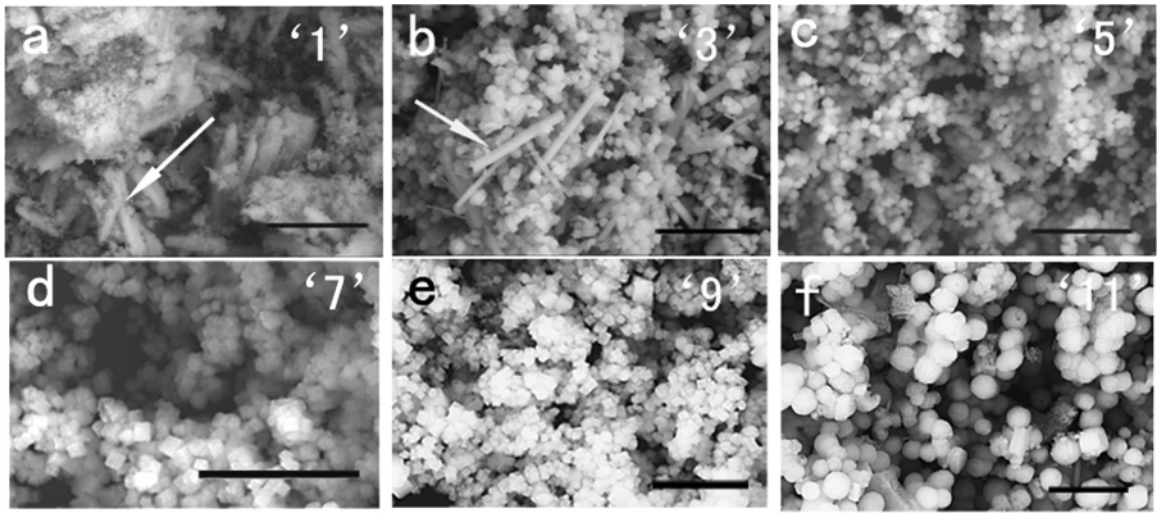

Figure 8. Time-dependent particle evolution. (a−f) SEM images of samples 1, 3, 5, 7, 9, and 11, respectively. Scale bar in each image = 1 μm.

at 220 °C, did not yield any crystalline $BaZrO_3$. Sample 2, quenched 10 min later at 270 °C, consisted of 21.7% $BaZrO_3$; small cubic particles, measuring ∼90 nm, were observed. From sample series 2−8, the weight percentage of $BaZrO_3$ increased dramatically from 21.7% associated with sample 2 (which had been prepared at 270 °C after 50 min of reaction time) to 96.1% associated with sample 7 (which had been synthesized at 720 °C after 140 min of reaction time). Overall data are summarized in Table 3.

Reaction at 720 °C yielded the best results in terms of sample purity. Over this particular sample set from 1 through 7, the observed particle size did not vary significantly (range of 90−100 nm), but the cube morphology predominated (Figure 7b). Increasing the overall reaction time further from 170 to 350 min (e.g., samples 8−11) not only increased the weight percentage of $BaZrO_3$ obtained to ∼100% but also basically tripled the observed particle sizes from ∼100 to >300 nm in diameter. Moreover, these latter samples possessed increasingly larger percentages of spherical particles.

All of these results agree well with the mechanism we proposed earlier for $BaZrO_3$ synthesis.[38] That is, upon heating of the initial mixture, the precursors dissolve into the resultant molten flux and gradually form $BaZrO_3$, which itself has a limited solubility. Upon attainment of a level of concentration supersaturation above the critical solubility (i.e., above the critical energy barrier) of $BaZrO_3$ required for the formation of nuclei, cubic particles are initially generated. Hence, increasing the annealing temperature has the practical effect of favoring the formation of $BaZrO_3$, thereby increasing its nucleation rate and generating a large quantity of initial cubic seed particles. This reasonable hypothesis (i.e., the formation of these seed particles) may explain why particles synthesized at higher temperatures at identical reaction times are actually smaller than those produced at lower temperatures (samples G−I). Moreover, because these initial cubic seed nuclei particles are likely to be below the critical particle size necessary for an in situ conversion, the implication is that particle transformation from cubes to spheres is not as favored at first.

That is, once nucleation begins, particle growth occurs simultaneously, as shown in Region A of Supporting Information Figure S8 (samples 2−8). The conversion of cubes to spheres also appears as a parallel process, upon attainment of a critical particle size for the cube precursors (Region B in Supporting Information Figure S8, samples 9−11). Overall, it is reasonable to assume that there is a critical threshold concentration required for the initial nucleation and formation of the cubes as well as a critical nucleus dimension for these cubes to acquire prior to their transformation into spheres. Growth and conversion trends converged for samples 9−11 with the formation of samples containing predominantly large spheres (>300 nm).

Conclusion

On the basis of the MSS of $BaZrO_3$ submicrometer-sized particles, the effects of different parameters, such as salt, surfactant, reaction temperature, reaction time, precursor type, amount of salt, heating/cooling rate, and molar precursor ratio, on the resultant product purity, size, shape, and morphology have been discussed. Among these various parameters, the selection of salt is likely the most important one because solubility and reactivity effects associated with the salt can very significantly alter the synthesis process as well as the resultant particle size and shape.

In general, the production of relatively high-quality $BaZrO_3$ samples was favored by high annealing temperatures, slow cooling rates, and overall long reaction times. In terms of optimal overall reaction conditions, uniform, crystalline, well-dispersed, and chemically homogeneous $BaZrO_3$ submicrometer-sized particles were obtained using BaC_2O_4 and ZrO_2 as precursors, NaOH/KOH as the molten reaction medium, a molar ratio of BaC_2O_4/ZrO_2/salt corresponding to 1:1:20, a heating rate of 5 °C/min, as well as a reaction temperature of 720 °C. Shorter annealing times (e.g., 30 min) coupled with higher cooling rates (e.g., 100 °C/min) favored the production of smaller-sized cubic particles. By contrast, longer annealing times (e.g., 60−210 min) and/or a slower cooling rate (5 °C/min) induced particle conversion from cubes to spheres and usually resulted in a mixture of cube and sphere morphological motifs. Either increasing the annealing time or slowing the cooling rate resulted in the formation of larger spherical particles. Most importantly,

we have shown that reliable size, shape, and composition control can be achieved in molten salt syntheses by judicious parameter selection.

Acknowledgment. We acknowledge the U.S. Department of Energy (DE-AC02-98CH10886) for facility and personnel support, as well as the National Science Foundation (DMII-0403859 and CAREER Award DMR-0348239) and the Alfred P. Sloan Foundation for PI support and experimental supplies, respectively. We also thank J. Huang and S. Chen (Boston College) as well as J. Quinn (SUNY Stony Brook) for assistance with microscopy.

Supporting Information Available: Figures S1−S8. This material is available free of charge via the Internet at http://pubs.acs.org.

CM071456J